

Analog MIMO RoC Passive Relay for Indoor Deployments of Wireless Networks

A. Matera, V. Rampa, M. Donati, A. Colamonic, A. F. Cattoni and U. Spagnolini

Abstract—Most of the indoor coverage issues arise from network deployments that are usually planned for outdoor scenarios. Moreover, the ever-growing number of devices with different Radio Access Technologies (RATs), expected for new 5G scenarios and to maintain compatibility with older cellular standards (mostly 3G/4G), worsen this situation thus calling for novel bandwidth-efficient, low-latency and cost-effective solutions for indoor coverage. To solve this problem, Centralized Radio Access Network (C-RAN) architectures have been proposed to provide dense and controlled coverage inside buildings. However, all-digital C-RAN solutions are complex and expensive when indoor layout constraints and device costs are considered. We discuss here an analog C-RAN architecture, referred to as Analog MIMO Radio-over-Copper (A-MIMO-RoC), that aims at distributing RF signals indoors over distances in the order of 50 m. The all-analog passive-only design presented here proves the feasibility of analog relaying of MIMO radio signals over LAN cables at frequency bandwidth values up to 400 MHz for multi-RAT applications. After asserting the feasibility of the A-MIMO-RoC platform, we present some experimental results obtained with the proposed architecture. These preliminary results show that the A-MIMO-RoC system is a valid solution towards the design of dedicated 4G/5G indoor wireless systems for the billions of buildings which nowadays still suffer from severe indoor coverage issues.

I. INTRODUCTION

5G networks [1] are already a reality: in 2020, according to [2], 96% of wireless data traffic will originate or terminate within a building, against 80% in 2016, with an exponential increase of indoor wireless market value. However, only few indoor commercial real estate have dedicated in-building cellular systems while most indoor areas are served by wireless networks originally designed and deployed for outdoor. This is the main reason to provide bandwidth-efficient, ultra-low latency and low-cost solutions to enhance indoor coverage. Centralized Radio Access Network (C-RAN) enables such an ambitious goal with full compatibility among different Radio Access Technologies (RATs) vendors, and still guaranteeing aggregate service reliability. Even if cell densification is the key enabler to cope with radio propagation limits, this will introduce unprecedented complex propagation scenarios, thus calling for a different approach in the way RAN resources and functions are allocated and handled. According to this, C-RAN, already deployed in current 4G networks, will surely

play a fundamental role also in 5G networks, even if it will need to be substantially redesigned to accommodate more demanding requirements. In 4G networks, Remote Radio Units (RRUs) and BaseBand Units (BBUs) communicates over a high-capacity link, namely the mobile FrontHaul (FH), that is usually implemented by fiber optic connections (Optical Transport Network). This architecture is designed to support streaming of digitized radio frequency (RF) signals according to specific digital streaming protocols e.g. the Common Public Radio Interface (CPRI) [3]. However, it is widely agreed that today available CPRI-based FH will hardly scale to the increased radio signal bandwidth foreseen by 5G networks, especially for multiple-antenna RRUs with massive MIMO constraints. This is due to the fact that Analog-to-Digital and Digital-to-Analog Converters (ADC/DAC) used in the RRUs, in addition to uncontrolled end-to-end latency, will also cause a severe bandwidth explosion, thus surpassing the capacity of current mobile FH links [4]. To overcome these limitations, new RAN architectures have been recently proposed with the aim of making the redistribution of RAN functionalities between BBUs and RRUs more flexible [5]. Even the CPRI group has proposed an enhanced version of the standard that includes intra-PHY functional splits [6].

Unlike digital RAN, Analog Radio-over-Copper (A-RoC) solutions [7], [8], [9] are able to loosen the FH requirements by simply substituting the conventional digital FH links with a fully analog transmission of RF signal between RRUs and BBUs using the ubiquitous cables used for fixed network deployments. A-RoC FH links not only completely bypass any bandwidth, latency and complexity issues due to digitization [10], but also reduce hardware costs, improve energy efficiency, and, above all, easily allow for synchronization among multiple decentralized RRUs, thus enabling MIMO joint-RRUs processing. In analog C-RAN, the RF analog-only functionalities are left in the RRUs, which become based only on low-complexity/low-cost analog components. RRU functionalities are thus limited to signal conversion to/from RF from/to Intermediate Frequency (IF) signals, and relaying, adaptation and equalization of IF signals to/from the BBUs according to the FH capabilities. Furthermore, the RRUs used in analog FH are protocol-independent and fully-bidirectional units, hence capable to transparently relay any RAT signal, which represents a fundamental step towards the wide-range heterogeneity promised by the 5G revolution. Analog Radio-over-Fiber (A-RoF) [11] is another promising analog FH technology able to provide high throughput links. However, due to its cost and complexity, it cannot compete against A-RoC for indoors and it will not be discussed here.

A. Matera, M. Donati, and U. Spagnolini are with DEIB, Politecnico di Milano: {andrea.matera,umberto.spagnolini,marcello.donati}@polimi.it.

V. Rampa (corresponding author) is with IEIIT, National Research Council of Italy (CNR): vittorio.rampa@ieiit.cnr.it

A. Colamonic is with ABC Progetti, Milano: armando.colamonic@tin.it.

A. Cattoni is with Keysight Technologies: andrea.cattoni@keysight.com.

This work has been partially funded by the TRIANGLE project, European Union Horizon 2020 Research and Innovation Programme, Grant No 688712.

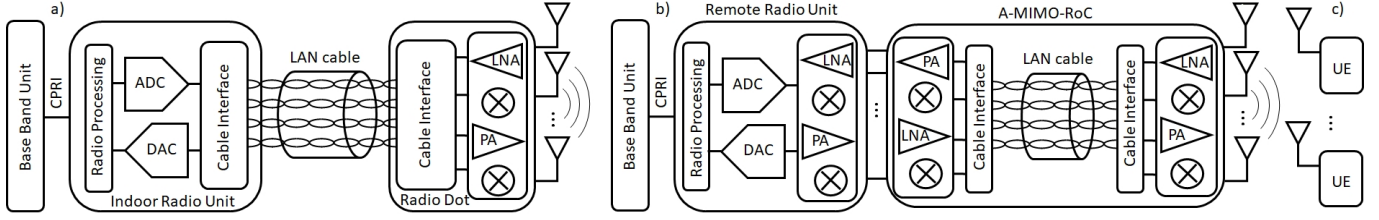


Fig. 1. Architectural comparison: a) Radio Dot connects the remote antennas with IRU and BBU; b) A-MIMO-RoC connects the remote antennas with the RRU; c) UEs are connected to a) or b) via the air interface.

Contributions: The contributions are three-fold: *i)* the proposal of an all-analog passive-only RF/IF hardware platform able to transparently transport independent wireless signals, having different bandwidth requirements, and even belonging to different RATs, *e.g.* LTE, WiMAX and WiFi, over off-the-shelf Cat-5/6/7 LAN cables; *ii)* the implementation of this platform with a fully-bidirectional scalable RF/IF architecture with limited cost and very low complexity; *iii)* the test and verification of the proposed platform to show that, for limited lengths of the LAN cables, it can be transparently used by any RF device to connect with remote RF antennas.

Organization: The A-MIMO-RoC architecture is shown in Sect. II while its signal model is described in Sect. III with some system-level simulations. Sect. IV deals with the validation of proposed architecture and shows some experimental results. Finally, conclusions are drawn in Sect. V.

II. SYSTEM ARCHITECTURE

The A-MIMO-RoC architecture presented here finds its roots in the A-RoC systems proposed by [7] for femto-cell systems where existing 4 twisted-pairs LAN cables were suggested to decouple PHY/MAC functionalities from RF units. The A-RoC concept has been extended to LTE networks in [12] using 6 twisted-pairs cables adopted in Digital Subscriber Line scenarios. However, both proposals restrict the cable bandwidth to a few tenths of MHz. The Radio Dot System [8], sketched in Fig. 1.a, partly overcame this problem while the A-MIMO-RoC architecture [13], [14] was able to relay multiple RATs MIMO signals over multi-pair copper-cables by filling the entire cable bandwidth for each pair. The feasibility of the proposed A-MIMO-RoC system has been shown in [15] by leveraging the end-to-end testing capabilities of the TRIANGLE testbed [16]. Fig. 1.b shows the generic block diagram of the A-MIMO-RoC architecture [13], [15] where the BBU communicates with the terminals (UEs) as in Fig. 1.c, through the RRU by using remote antennas. Unlike the Radio Dot System [8], where the RRU is split into two parts, namely the Radio Dot and the Indoor Radio Unit (IRU), the proposed A-MIMO-RoC architecture does not have direct access to the BBU control signals. To limit the cost, simplify the design and increase its applicability, the A-MIMO-RoC architecture is composed by two identical units called LAN-to-Coax Converters (L2CCs) that take the RF signals directly from the RRU (not the BBU) and convert them from RF to IF and vice versa to connect with the remote RF antennas by using a LAN cable. While in [8] the twisted-pairs of the LAN cable carry also control, signalling, synchronization lines and

power, the bi/directional L2CC blocks of Fig. 1.b are used only to adapt, convert RF, and equalize IF signals. The A-MIMO-RoC prototype is implemented using only passive devices in the RF/IF signal path with no LNAs (Low Noise Amplifiers), PAs (Power Amplifiers) or any active filter/mixer as in the generic architecture of Fig. 1.b. Active devices could be used in the RF/IF paths but this would imply a more complex and costly implementation. Each L2CC is composed by L identical signal slices (Fig. 2 and 3) and each l -th twisted-pair is assigned to the l -th signal slice with $l = 1, \dots, L$. Assuming $N = ML$ RF signals (it is $N = 8, M = 2, L = 4$ in our implementation), the l -th signal slice takes M RF signals, that are applied to the RF ports $TRX_{M(l-1)+1}$ up to TRX_{Ml} . Then *i)* each signal slice converts the RF signals into M IF ones by using the doubled-balanced diode-based mixers MCA-35LH+ from Mini-Circuits. The Phase-Locked Loop (PLL) synthesizer ADF4351, from Analog Devices, and the amplifier SKY65014-70LF, from Skyworks Solutions, are used for each Local Oscillator (LO) stage. The M IF-converted signals are then: *ii)* combined in a single IF line, using a resistive M-way combiner, and: *iii)* fed into the passive cable equalizer (split into two identical RC filters) that is tuned for fixed cable lengths (Sect. IV). Finally: *iv)*, the balun ADT2-1T+, from

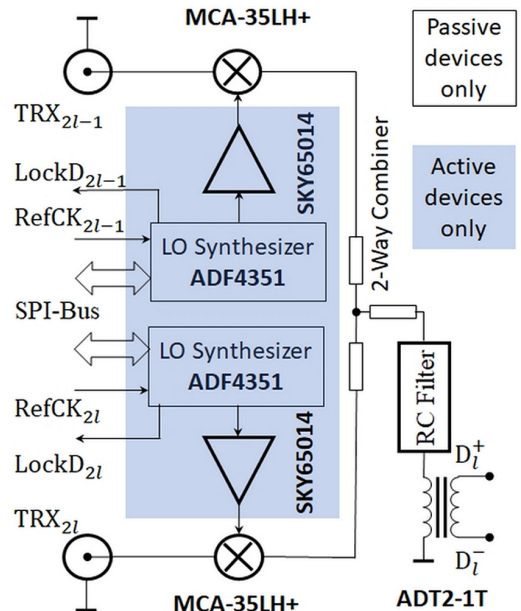


Fig. 2. Detailed functional scheme of the l -th signal slice of the L2CC box shown in Fig. 1.b and 3. IC part numbers specify the devices used.

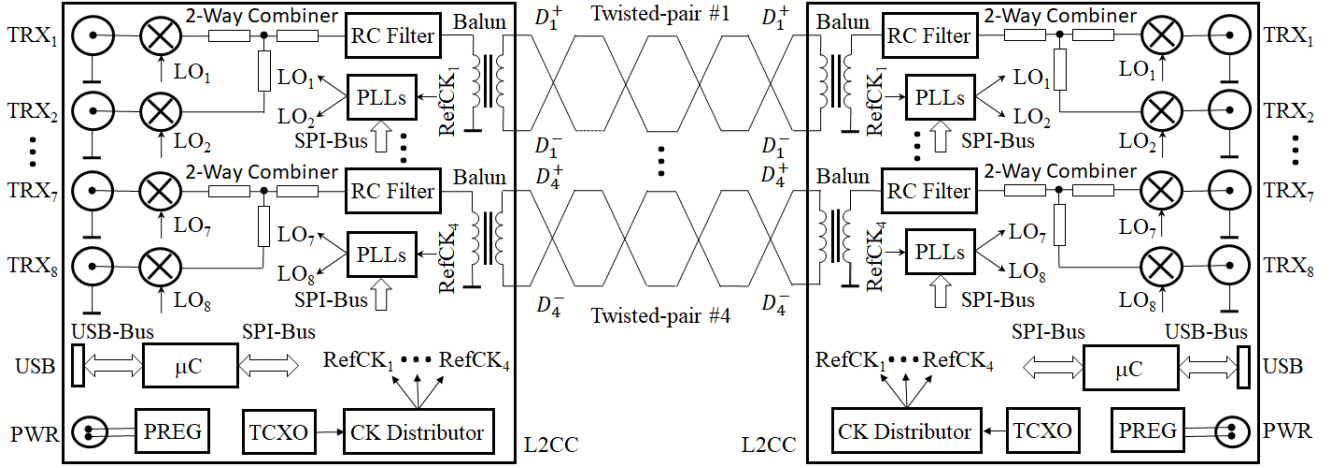


Fig. 3. Block diagram of the all-analog A-MIMO-RoC system of Fig.1.b. The L2CC boxes are composed by: *i*) L signal slices, detailed in Fig. 2; *ii*) the clock generator and distributor; *iii*) the microcontroller (μC) and *iv*) the power regulators (PREG). In this implementation, it is $N = 8$, $M = 2$, and $L = 4$.

Mini-Circuits, is used to adapt the equalizer impedance (50Ω , unbalanced) to the twisted-pair one (100Ω , balanced). Another L2CC box (Fig. 3) is then employed to convert IF signals back to RF just reversing the previous operations without using any control signal: Uplink (UL) and Downlink (DL) modes are thus identical. LO frequencies are statically assigned during start-up by programming the PLLs using the microcontroller PIC16F1789 (μC) from Microchip Technology. LOs can be also dynamically configured through remote commands from the USB interface by using the internal SPI Bus. The clock generator feeding the PLLs is composed by the 10 MHz TCXO (Temperature-Compensated Crystal Oscillator) CW837CT-ND from Connor-Winfield (frequency stability ± 50 ppb), while the clock distributor is the IDT 83908I-02. To avoid non-linearity effects, the recommended maximum input power for each RF port is set to 0 dBm while +5 dBm is the maximum applicable RF input power. The current L2CC implementation shown in Fig. 3 is composed by a motherboard that holds the power regulators (PREG), the μC , the USB interface, the clock generator (TCXO), clock distributor (CK Distributor), and $L = 4$ daughter-boards that implement the signal slices. Scalability is obtained by *i*) increasing the number L of daughter-boards, if LAN cables with $L > 4$ twisted-pairs are used, by adding more clock lines; *ii*) increasing the number $M > 2$ just adding more mixers and combiners. Theoretically, the proposed platform could be employed in the mm-Wave bands of the 5G New Radio Frequency Range 2 (FR2) allocation. However, transmission of wide-band non-OFDM signals is strongly impaired by the LAN cable characteristics and full active cable equalization must be implemented (Sect. IV). Presently, the high cost of current mm-Wave devices and their limited performances restrict the applicability of the proposed passive architecture to the FR1 bands only. Finally, Tab. I shows the main differences between available C-RAN architectures where PoE indicates Power over Ethernet and PO means Propagation Only due to the delay of the analog and/or optical components. Moreover, unlike A-RoC systems [8], [12], the SF2SF2 feature allows us to use M signals/pair at a time (e.g., for MIMO) not only 1 signal/pair.

TABLE I
COMPARISON OF MAIN FEATURES OF VARIOUS C-RAN SYSTEMS.

System	CPRI [3]	A-RoF [11]	A-RoC [8], [12]	A-MIMO-RoC [15]
BW increment	$\times 18 \div 30$	$\times 1$	$\times 1$	$\times 1$
Latency	$\sim 100 \mu s$	PO	PO	PO
Complexity	High	High	Low	Very low
RF antennas	$N \gg 1$	$N \gg 1$	$N \leq L$	$N \leq ML$
Infrastructure cost	Very high	Very high	Very low	Very low
Power supply	External	External	PoE/Ext	PoE/Ext

III. SIGNAL MODEL

As shown in Fig. 4, the in/out RF signals are represented by the $N \times 1$ band-pass vectors \mathbf{s} and \mathbf{s}' with central frequencies $\mathbf{f}_0 = [f_n^{(0)}]$ and $\mathbf{f}'_0 = [f'_n{}^{(0)}]$, respectively. Assuming initial zero phase terms, $[s_n(t)]$ and $[s'_n(t)]$ as baseband representations of \mathbf{s} and \mathbf{s}' , it is $\mathbf{s} = [\Re\{s_n(t) \exp(2\pi j f_n^{(0)} t)\}]$ and $\mathbf{s}' = [\Re\{s'_n(t) \exp(2\pi j f'_n{}^{(0)} t)\}]$ while the signal model is

$$\mathbf{s}' = \mathbf{A} \mathbf{s} + \mathbf{B} \mathbf{w}_c \quad (1)$$

with matrices $\mathbf{A} = \mathbf{M}_U \mathbf{\Pi}_b^T \mathbf{H} \mathbf{\Pi}_b \mathbf{M}_D$ and $\mathbf{B} = \mathbf{M}_U \mathbf{\Pi}_b^T \mathbf{H}_b$ of size $N \times N$ and $N \times L$, respectively. Noise effects are represented by the $L \times 1$ Gaussian vector \mathbf{w}_c while the $N \times N$ matrices $\mathbf{M}_D = \text{diag}[\cos(2\pi j f_n^{(D)} t)]$ and $\mathbf{M}_U = \text{diag}[\cos(2\pi j f_n^{(U)} t)]$ represent down- and up-conversion that are driven by the $N \times 1$ LO frequency vectors $\mathbf{f}_D = [f_n^{(D)}]$ and $\mathbf{f}_U = [f_n^{(U)}]$, respectively. The matrix $\mathbf{H} = \mathbf{H}_b \otimes \mathbf{H}_c \otimes \mathbf{H}_b$

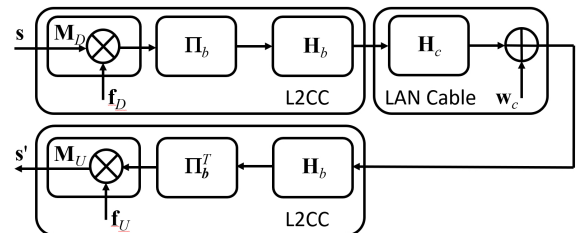


Fig. 4. DL/UL signal model the A-MIMO-RoC platform.

of size $L \times L$ includes the filtering effects due to \mathbf{H}_c , imputable to each twisted-pair of the LAN cable, and those due to \mathbf{H}_b , introduced by the mixer, balun and cable equalizer. Band inversion is avoided by proper programming the LO frequencies of the corresponding signal slices. Likewise, also due to the filtering effects introduced by \mathbf{H}_b and \mathbf{H}_c , IF images are eliminated by selecting the appropriate LO frequencies. Theoretically, the corresponding LO signals are set to the same frequency $f_D = f_U$. In practice, fine LO tuning can be used to reduce frequency errors between in/out RF signals (Sect. IV). To mitigate the LAN cable impairments, a key feature of the A-MIMO-RoC architecture is the mapping of the RF signals of each RRU antenna into a combination of twisted-pair/IF allocations, namely Space-Frequency to Space-Frequency (SF2SF) mapping [13]. Here, SF2SF mapping is split into Space and Frequency Mappings: the $L \times N$ binary matrix $\mathbf{\Pi}_b = [(\pi_b)_{l,n}]$ defines the Space Mapping matrix that implements only the space allocation strategy. It is statically assigned by selecting the chosen RF cable connections since the signal slice/twisted-pair association is fixed. In fact, the RF signals applied to the TRX_{2l-1} and TRX_{2l} ports are converted, mixed together and then assigned to the l -th signal slice that is wired to the l -th twisted-pair: $\forall n = 1, \dots, N$ and $\forall l = 1, \dots, L$, each binary element $(\pi_b)_{l,n}$ is set to 1 iff the n -th RF signal is connected to the l -th signal slice, otherwise it is set to 0. Frequency Mapping is dynamically performed by selecting the specific LO frequencies $f_D = [f_n^{(D)}]$ and $f_U = [f_n^{(U)}]$.

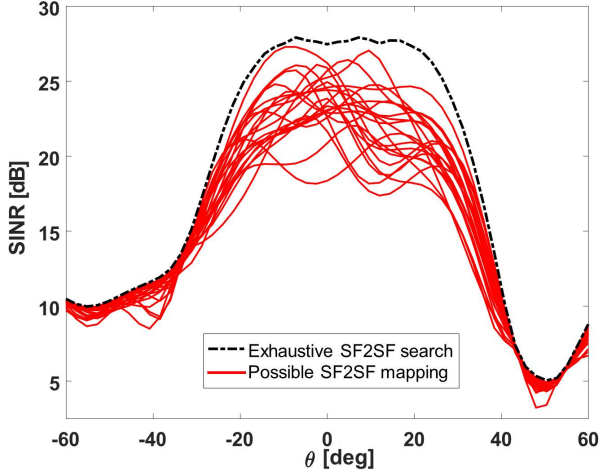


Fig. 5. SINR vs. θ : exhaustive search vs. some possible SF2SF mappings.

Adopting the model (1) and the ideal interference scenario shown in Sect. IV of [17] with one active UE, two interfering UEs, 20 MHz LTE signals with QAM modulation, $L = 4$ twisted-pairs and $N = 8$ antennas beamforming at the BBU, Fig. 5 shows the SINR (Signal to Interference-plus-Noise Ratio) vs. θ (UE steering vector). Uniform linear array and Minimum Variance Distortionless Response (MVDR) beamforming are also assumed. The optimal SF2SF mapping is shown with possible specific mapping choices. It is apparent that the SINR dispersion is ~ 10 dB from the exhaustive search of the optimum mapping. For the experimental platform, the optimal choice of the SF2SF values are set up according to

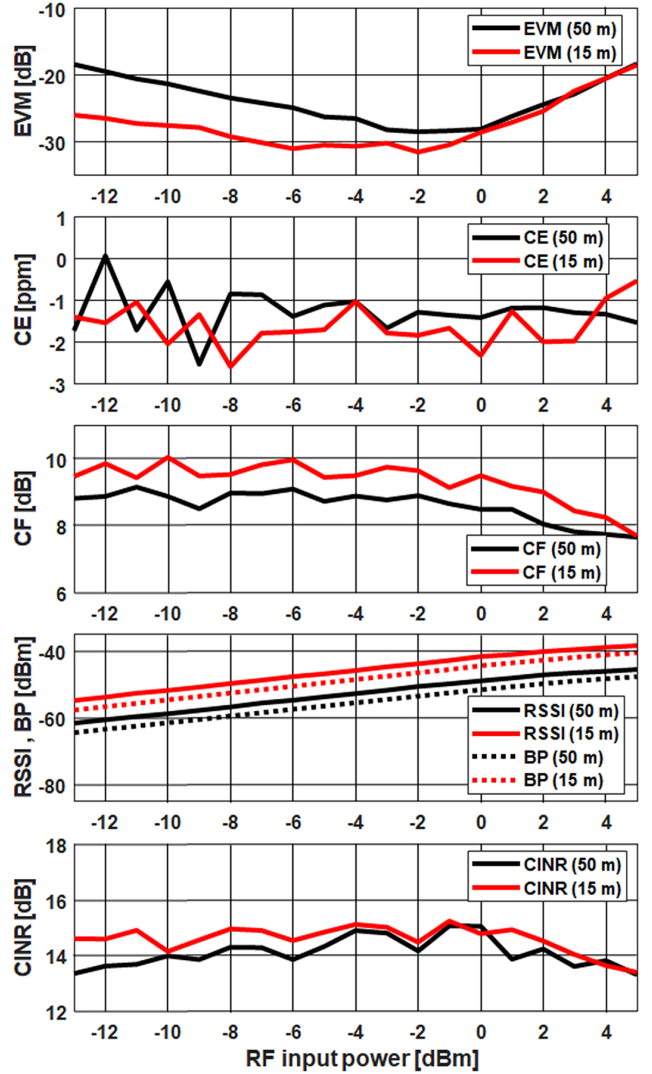


Fig. 6. From the top: EVM [dB], CE [ppm], CF [dB], RSSI [dBm], BP [dBm] and CINR [dB] measurements with WiMAX signals. Both results for 15 m and 50 m long LAN cables are considered.

the evaluated end-to-end performances (Sect. IV).

IV. MEASUREMENTS AND EXPERIMENTAL RESULTS

The A-MIMO-RoC performances with LAN cables of different type and length (Cat-5, 15 m and Cat-5e, 50 m) are evaluated here when connected to lab instruments and real communication devices. For lab measurements, we used a R&S Vector Signal generator SMJ100A with WiMAX/LTE options and a R&S FSG Spectrum Analyzer with WiMAX option only. Fig. 6 shows the following WiMAX test results with 15 m and 50 m cables: Error Vector Magnitude (EVM), Clock Error (CE), Crest Factor (CF), Received Signal Strength Indicator (RSSI), Burst Power (BP), and Carrier to Interference-plus-Noise Ratio (CINR). The TRX₁ port of the first L2CC is tied to the R&S SMJ100A generator while the TRX₁ port of the other L2CC is connected to the R&S FSG Analyzer. The WiMAX signal has $f_1^{(0)} = 2.63$ GHz while both PLL synthesizers are configured to generate LO₁ frequencies $f_1^{(D)} = f_1^{(U)} = 2.77$ GHz corresponding to an

IF value of 140 MHz. WiMAX bursts are generated with the following specs: IEEE 802.16-2004 8 ms TDD DL burst, guard time 1/4, roll-off factor 0.1, Modulation and Coding Scheme (MCS) set to 16-QAM rate 3/4, nominal bandwidth 7 MHz, 16 sub-channels, and long preamble. From EVM, BP, CF and CINR measurements, it is apparent the non-linearity effect, mostly due to the mixers, that limits the RF input power larger than ≈ 0 dBm for both cables. For RF input power values lower than -7 dBm (50 m) and -15 dBm (15 m), the signal to noise ratio decreases thus increasing the EVM over the WiMAX limit of -25 dBm for the selected MCS configuration. RSSI measurements highlight the effects due to both LAN cable lengths and passive devices that introduce ~ 50 dB of end-to-end attenuation for the 50 m cable and ~ 42 dB for the 15 m one. Carrier Frequency Error (CFE), not shown in Fig. 6, is almost constant with small variations in the range $[-4190, -4177]$ Hz (50 m) and $[-3559, -3475]$ Hz (15 m) due to the tuning mismatch between the corresponding LO lines $f_1^{(D)}$ and $f_1^{(U)}$ generated by different PLL synthesizers. CFE can be almost eliminated by tuning both LO frequencies. The good frequency stability of the clock generation/distribution stages is also confirmed by the CE tests whose values are in the range of $[-2.5, +0.1]$ ppm for both cables. Moreover, phase noise measurements at the LO₁ lines, not shown here, indicate a residual PM of 1.21 deg and a RMS jitter of 1.4 ps. After LO calibration, the CFE can be reduced below the ± 0.1 ppm LTE limit. For end-to-end evaluation, LTE signals have been generated by a Keysight UXM RAN emulator with ETSI Static MIMO channel [16]. Fig. 7 shows the throughput results in Mbps, for MIMO LTE tests (TDD mode, $BW = 5$ MHz, TM3 mode, B38 band, TX power at -20 dBm, 2x2 MIMO) at different IF frequencies (75, 175, and 400 MHz) for different MCS indexes. The 2x2 MIMO LTE signals have been relayed over two twisted-pairs but at the same cable IF, and thus interfering with each other. Nevertheless, the performance loss is negligible for almost all MCS and IF values. Fig. 7 depicts the throughput results when a WiFi signal at $IF = 50$ MHz is added to the LTE one at $IF = 175$ MHz. A commercial WiFi access point has been used to handle the WiFi traffic (IEEE802.11n, $BW = 20$ MHz, 2x2 MIMO, Channel 1, TX power at 0 dBm) and the first two twisted-pairs have been used to relay the 2x2 MIMO signals. Up to MCS 13 (16QAM) the effect of the WiFi signal is almost negligible while it is more pronounced for higher MCS values. These effects are mostly due to the fact that the LTE UE operates close to its sensitivity threshold for the high attenuation introduced by the LAN cable. With shorter LAN cables with length in the order of 15 m \div 20 m and attenuation about 20 dB \div 25 dB, the overall system attenuation problem is no more an issue (see EVM values in Fig. 6). Even if passive implementation simplifies the design, experimental results for long cables applications and new scenarios in the 5G mm-Wave bands suggest the use of active devices in the signal path. Finally, additional test results are presented in [15].

V. CONCLUSIONS AND FUTURE WORKS

This paper presents the architecture and preliminary results showing the feasibility of the A-MIMO-RoC system. It

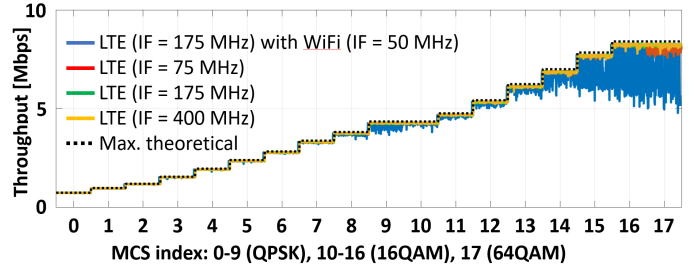


Fig. 7. Throughput [Mbps] of end-to-end tests for different protocols (LTE, WiFi), MCS indexes (0-17), and IF values (50, 75, 175 and 400 MHz).

is able to transparently transport multi-RAT MIMO signals over a single LAN cable by a judicious exploitation of the bandwidth of the interconnecting LAN cable up to several hundreds of MHz. Performance degradation experienced for high modulation schemes is mainly due to the high attenuation introduced by the system caused by the full-passive analog implementation. However, with shorter LAN cable length the overall system attenuation can be reduced to a tolerable level.

REFERENCES

- [1] M. Agiwal, et al., "Next Generation 5G Wireless Networks: A Comprehensive Survey," IEEE Comm. Surveys & Tutorials, vol. 18, no. 3, pp. 1617-1655, 2016.
- [2] Commscope, "Wireless in Buildings: What Building Professionals Think," CO-11043-EN (02/16), 2016.
- [3] Ericsson AB, et al., "CPRI Specifications V7.0 - Common Public Radio Interface (CPRI); Interface Specification," Oct. 9, 2015.
- [4] D. Wubben, et al., "Benefits and impact of cloud computing on 5G signal processing: Flexible centralization through cloud-RAN," IEEE Signal Processing Magazine, vol. 31, no. 6, pp. 35-44, Nov. 2014.
- [5] J. Bartelt, et al., "Fronthaul and backhaul requirements of flexibly centralized radio access networks," IEEE Wireless Communications, vol. 22, no. 5, pp. 105-111, Oct. 2015.
- [6] CPRI Cooperation, "CPRI Specifications eCPRI 2.0," 2019.
- [7] J. Gambini, et al., "Wireless over cable for femtocell systems," IEEE Communications Magazine, vol. 51, no. 5, pp. 178-185, May 2013.
- [8] C. Lu, et al., "Connecting the dots: small cells shape up for high-performance indoor radio," Ericsson Review, vol. 91, no. 12, 2014.
- [9] F. Tonini, et al., "Radio and transport planning of centralized radio architectures in 5G indoor scenarios," IEEE Journal on Selected Areas in Communications, vol. 35, no. 8, pp. 1837-1848, Aug. 2017.
- [10] D. Acatauassu, et al., "Coaxial Networks for 5G Fronthaul," Proc. of the IEEE 23rd International Workshop on Computer Aided Modeling and Design of Communication Links and Networks (CAMAD'18), pp. 1-6, Barcelona, Sep. 17-19, 2018.
- [11] D. Wake, et al., "Radio over fiber link design for next generation wireless systems," Journal of Lightwave Technology, vol. 28, no. 16, pp. 2456-2464, Aug. 2010.
- [12] E. Medeiros, et al., "Crosstalk mitigation for LTE-over-copper in downlink direction," IEEE Communications Letters, vol. 20, no. 7, pp. 1425-1428, Jul. 2016.
- [13] A. Matera, et al., "Analog MIMO Radio-Over-Copper Downlink With Space-Frequency to Space-Frequency Multiplexing for Multi-User 5G Indoor Deployments," IEEE Transactions on Wireless Communications, vol. 18, no. 5, pp. 2813-2827, May 2019.
- [14] S. H. R. Naqvi, et al., "A Novel Distributed Antenna Access Architecture for 5G Indoor Service Provisioning," IEEE Journal on Selected Areas in Communications, vol. 36, no. 11, pp. 2518-2527, Nov. 2018.
- [15] A. Matera, et al., "Analog MIMO Radio-over-Copper: Prototype and Preliminary Experimental Results," Proc. of the 16th Intl. Symp. on Wir. Comm. Sys. (ISWCS'19), pp. 1-5, Oulu, Aug. 27-30, 2019.
- [16] A. D. Zayas, et al., "TRIANGLE: A Platform to Validate 5G KPIs in End to End scenarios," Proc. of the IEEE 23rd International Workshop on Computer Aided Modeling and Design of Communication Links and Networks (CAMAD'18), pp. 1-7, Barcelona, Sep. 17-19, 2018.
- [17] A. Matera, et al., "Space-Frequency to Space-Frequency for MIMO Radio over Copper," IEEE Intl. Conf. on Comm. (ICC'17), Paris, 2019.